CHEMISTRY OF MATERIALS

pubs.acs.org/cm

Article

Hypersensitivity of the Glass Transition to Pressure History in a Metal−Organic Framework Glass

Ang Qiao,[▽] Søren S. Sørensen,[▽] Malwina Stepniewska, Christophe A. N. Biscio, Lisbeth Fajstrup, Zhu Wang, Xianghua Zhang, Laurent Calvez, Ivan Hung, Zhehong Gan, Morten M. Smedskjaer,* and Yuanzheng Yue*

Cite This: *Chem. Mater.* 2022, 34, 5030−5038

Read Online

ACCESS | Metrics & More | Article Recommendations | Supporting Information

ABSTRACT: Metal−organic framework (MOF) glasses feature numerous unique properties and potential applications, but many fundamental questions remain unanswered, especially concerning their glass transition. Here, we report a discovery about ZIF-62 glass (a typical MOF glass), namely, the hypersensitivity of its glass transition to pressure history. Specifically, upon quenching the ZIF-62 melt under a modest pressure of 60 MPa, the derived glass exhibited a significantly lower glass transition temperature (T_g) than the glass formed under ambient pressure. The sensitivity parameter of T_g to pressure for ZIF-62 glass is much higher than that of other glass systems, including polymer glasses that typically feature a huge increase in T_g upon compression. The origin of the hypersensitivity of T_g to pressure history was revealed by structural analyses, positron annihilation lifetime spectroscopy, and molecular dynamics simulations. We found that the medium-range structure change induced the drop in T_g.

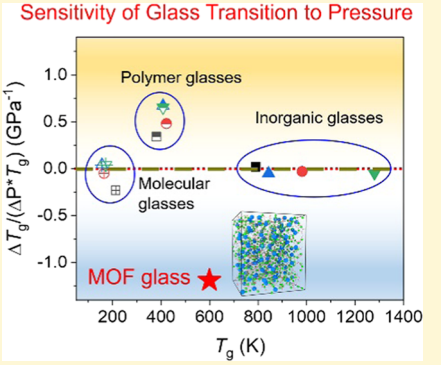

INTRODUCTION

The structure, dynamics, and macroscopic properties of disordered materials such as glasses can be tuned by varying the pressure.[1−6] Numerous fascinating phenomena, e.g., structural densification,[1,2,4] polyamorphism,[6] and variations in glass transition behavior,[3,5] have been observed in oxide, chalcogenide, and metallic glasses when applying a high pressure during melt-quenching. Furthermore, applied pressure significantly influences the glass transition temperature (T_g), where both negative and positive relationships between T_g and pressure have been observed, depending on the glass composition.[3,5,7−10] Among them, polymer glasses are known to feature an especially pronounced sensitivity of T_g to pressure.[7,8] However, to the best of our knowledge, it has not been explored how the glass transition of the family of metal−organic framework (MOF) glasses[11−13] responds to their pressure history. Such exploration will contribute to the understanding of the glass transition and glass formation mechanism of MOFs, as well as to designing new types of MOF glasses.

Although an increasing number of hybrid glasses are currently being discovered,[14−16] the majority of the studies on three-dimensional MOF glasses are based on the zeolitic imidazolate frameworks (ZIFs), which are a subset of MOFs. ZIFs feature a zeolite-like framework structure, consisting of metal−ligand tetrahedra connected by coordination bonds.[17] When subjected to a high pressure, the crystalline ZIFs can undergo rich polymorphic transitions by converting to novel crystalline and amorphous phases.[18,19] Similar to vitreous silica, ZIF glasses are characterized by a fully polymerized structure, i.e., completely corner-shared metal−ligand tetrahedral network.[20] However, for a typical ZIF, e.g., ZIF-62 ($Zn(Im)_{1.75}(bIm)_{0.25}$, where Im is imidazolate and bIm is benzimidazolate), the size of the Im/bIm ligand (length of Im ∼4.0 Å) is much larger than that of the ions bonded to the central ion in non-MOF tetrahedral networks (e.g., the length of the Si−O bond is 1.6 Å). The large size of the ligands causes significant steric hindrance, restricting migration and rearrangement of the structural species (such as Zn, Im, and bIm) in ZIF-62 into an ordered state during melt-quenching, and hence, ZIF-62 exhibits ultrahigh glass-forming ability.[13] Recently, a high degree of short-range disorder in addition to the typical medium- and long-range disorder has been observed in ZIF-62 and ZIF-4 glasses compared to their parent crystals based on ultrahigh-field ^{67}Zn magic-angle-spinning (MAS) nuclear magnetic resonance (NMR) measurements.[21] Yet, despite some progress in understanding the structure and dynamics of melt-quenched MOF glasses, the following key question still needs to be answered: How does the microstructure affect the glass transition in MOF glasses?

Received: January 31, 2022
Revised: May 10, 2022
Published: May 23, 2022

Revealing the atomic-scale origin of the glass transition is one of the greatest challenges in condensed matter science, due to the difficulty in probing structural changes caused by the glass transition. From thermodynamic and kinetic perspectives, several classical theories and models of the glass transition have been developed, e.g., theories of free volume, configurational entropy, and mode coupling, as well as energy landscape and kinetically constrained models.[22] From a chemical and microstructural perspective, for organic glasses, T_g is affected by the degree of crosslinking of the molecular chains,[23] but for oxide glasses, T_g is determined by the average bond strength and degree of network polymerization.[22] However, these theories for the glass transition are not fully applicable to MOF glasses due to the significant structural differences between MOF glasses and other glass systems (inorganic, organic, metallic). As such, we note that the MOF glass systems involve not only the network structure but also the framework structure with subnanometer pores, which is absent in other glass systems. To study the glass transition of MOF glasses, we here investigate the dependence of the T_g value of a selected MOF glass (ZIF-62 glass) on the isostatic pressure applied during melting above T_g and subsequent quenching, i.e., on its pressure history.

Specifically, we densified ZIF-62 glass powder using the spark plasma sintering (SPS) method at various pressures and temperatures. By doing so, the densified MOF glass structure was frozen and ZIF-62 glass samples with different pressure histories were obtained for subsequent characterizations. We used differential scanning calorimetry (DSC) to detect the glass transition event and to determine T_g. We also annealed the compressed ZIF-62 glasses at ambient pressure to trace the responses of their T_g, hardness, and density values to structural densification and relaxation. The changes in short- and medium-range (SR and MR) structures of the compressed and uncompressed ZIF-62 glasses were probed using ultrahigh-field ^{67}Zn MAS NMR, Raman, and X-ray photoelectron spectroscopy (XPS), whereas the evolution of the sub-nano pore size was observed using positron annihilation lifetime spectroscopy (PALS). The atomistic rearrangement induced by pressure was also investigated by reactive molecular dynamics (MD) simulations and persistent homology analyses. We finally revealed the correlation between the microstructure and the glass transition behavior, and then discussed the mechanism of the pressure-induced variation in T_g.

EXPERIMENTAL SECTION

Synthesis. *Preparation of ZIF-62 Crystals and Glasses.* ZIF-62 crystals were synthesized using the same methodology as given in ref 13. Subsequently, the crystalline ZIF-62 powder was melted and quenched to a glass state in a tube furnace, using an inert argon atmosphere. To do so, the crystal powder was first heated to 733 K (above its melting point of about 693 K) at 10 K min^{-1}, followed by 5 min isothermal heating, before being naturally cooled to room temperature. The obtained melt-quenched ZIF-62 bulk glass was crushed and ground to obtain powder to be used as starting material for the SPS-based densification. Meanwhile, the melt-quenched (MQ) ZIF-62 bulk glass was also used as an object of study.

Preparation of ZIF-62 Bulk Glass by SPS. The ZIF-62 glass sintering process was performed under vacuum on an HP-D 10 SPS instrument (FCT System GmbH). Around 0.15 g of glassy ZIF-62 powder samples were filled into graphite dies (10 mm in diameter), and a K-type thermocouple was inserted centrally in a hole in the wall of the die. The process chamber was evacuated, and the temperature was raised at a rate of 50 K min^{-1} by resistive heat generated from passing a pulsed direct current (max. 0.35 kA, 4.65 V) through the graphite parts. After 2 min dwelling time, the samples were cooled at approximately 50 K min^{-1}. In this work, one series of ZIF-62 glass samples were sintered at different temperatures (583, 593, or 603 K) under a pressure of 60 MPa, while the other series was prepared at 593 K under different pressure (40, 50, or 60 MPa). These synthesis conditions are summarized in Table S1. The sample named "SPS glass-1" (sintered at 593 K under 60 MPa) is used as a standard sample to compare with the MQ glass. It should be mentioned that there was a temperature difference of 3 K between the glass sample and the temperature sensor. The above-mentioned sintering temperatures refer to those that were estimated based on the temperature gradient.

Measurements. The DSC characterizations for all of the samples were conducted using a Netzsch STA 449 F1 instrument. The samples were placed in a platinum crucible situated on a sample holder in the DSC at room temperature. The samples were held for 5 min at an initial temperature of 313 K, then heated at 10 K min^{-1} to 633 K, and then cooled back to 473 K at 10 K min^{-1}. After natural cooling to room temperature, the second and third upscans were performed using the same procedure. To determine the isobaric heat capacity (C_p) of the samples, both baseline (blank) and a reference sample (sapphire) were measured.

The phase structure of the prepared samples was confirmed by powder X-ray diffraction (XRD) method using a Panalytical Empyrean X-ray diffractometer operating at 45 kV and 40 mA, with Cu Kα radiation (λ = 1.5418Å).

The density of glasses at room temperature (23.1 °C) was measured according to Archimedes' principle with ethanol as the soaking solution. Each sample was measured 10 times to obtain the average density value and the error range.

The hardness of samples was measured using Vickers indentation (CB5000, Nanovea) with 0.49 N loading. The surface of the samples was polished to an optical finish prior to measurements. The loading rate was set to ascertain 6 s loading time (9.8 N min^{-1}) and a 15 s dwell was applied at the highest load.

The composition of the samples was measured by liquid ^{1}H NMR. Digested samples (in a mixture of DCl (35%)/D_2O (0.1 mL) and dimethyl sulfoxide (DMSO)-d_6 (0.5 mL)) of desolvated ZIF-62 samples (about 6 mg) were measured on a Bruker Avance III 600 MHz spectrometer at 293 K. Chemical shifts were referenced to the residual proton-solvent signals of DMSO-d_6. The spectra were processed with the MestreNova Suite.

Raman spectra were recorded using a Thermo Nicolet, Nexus Spectrometer with a YAG:Nd laser (1064 nm). A typical power of 0.1 W was used for recording spectra in the range of 100−2000 cm^{-1}.

X-ray photoelectron spectroscopy (XPS) measurements were performed by an ESCALAB 250Xi X-ray photoelectron spectrometer using Al K_α radiation. The spectra were calibrated by referencing the binding energy of carbon (C 1s, 284.6 eV).

The ^{67}Zn magic-angle spinning nuclear magnetic resonance (MAS NMR) spectra for both the MQ and SPS ZIF-62 glasses were conducted at the National High Magnetic Field Laboratory (NHMFL) using 3.2 mm magic-angle spinning probes and Bruker Avance NEO consoles. The PALS measurements were performed using an identical sample analysis methodology to that reported previously.[24] See the details of both measurements in Supporting Methods.

MD Simulations. *Glass Preparation.* Glasses were prepared using a ReaxFF force field as introduced in ref 25 and following the adapted procedure of ref 26. All simulations were performed in LAMMPS.[27] The method is summarized in the following. First, an initial unit cell of ZIF-62 (as obtained from ref 19) was replicated into a 2 × 2 × 2 supercell of 2368 atoms. Then, structures were energetically minimized and relaxed at 10 K for 7.5 ps using a Berendsen thermostat before heating to 300 K at 232 K ps^{-1}, all performed in the NPT ensemble at 0.1 MPa. Now, the pressure was either maintained at 0.1 MPa or increased to 60 MPa during another 12.5 ps of simulation at 300 K. This was followed by heating to 1500 K at 24 K ps^{-1} and subsequent cooling at a similar rate under either 0.1 MPa or 60 MPa of isostatic pressure. This is significantly longer than in the

https://doi.org/10.1021/acs.chemmater.2c00325
Chem. Mater. 2022, 34, 5030−5038

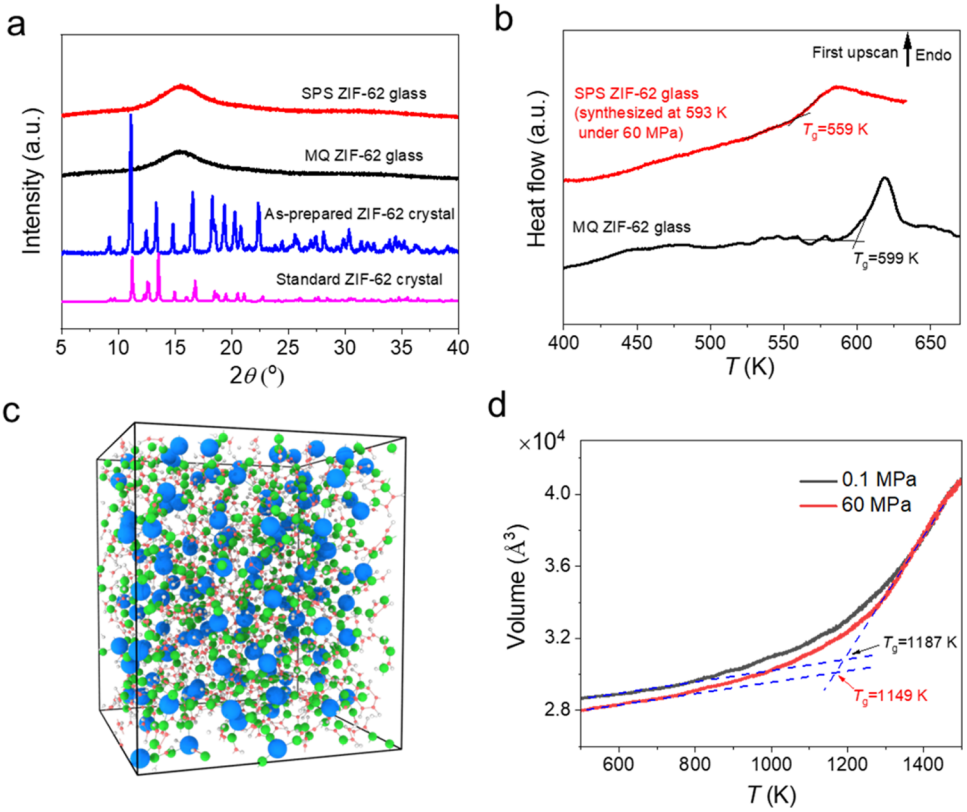

Figure 1. (a) X-ray diffraction patterns of standard ZIF-62 crystal, ZIF-62 crystal prepared by the solvothermal method, and ZIF-62 glasses synthesized via ambient pressure melt-quenching (MQ) and 60 MPa spark plasma sintering (SPS). (b) DSC upscan curves of ZIF-62 glasses obtained by MQ under ambient pressure and SPS at 593 K under 60 MPa pressure, showing the difference in glass transition temperature (T_g). (c) Atomic snapshot of simulated ZIF-62 glass structure under ambient pressure from reactive MD simulations. Atoms are colored red (carbon), gray (hydrogen), green (nitrogen), and blue (zinc). (d) Temperature dependence of the average volume of 20 MD-simulated structures at each pressure, during a heating procedure from 300 to 1500 K. The dashed lines represent linear fits to the V vs T data below and above T_g.

original work of ref 25 to allow for more atomic movement. We note that decreasing the heating rate and/or allowing for an isotherm at 1500 K will eventually cause the simulation box to evaporate. As such, the used approach is a compromise between allowing for more atomic movement while keeping the system in the molten state. In a separate simulation, we calculated the mean-square-displacement (MSD) for the components at 1500 K, finding all of the atoms to first show typical liquid behavior (i.e., linearly increasing MSD with increasing time), before eventually showing divergent behavior due to evaporation. Finally, the glasses were relaxed for 12.5 ps while relieving the applied pressure to 0.1 MPa before a final of 6.25 ps of statistical averaging in the NVT ensemble. All simulation steps used a timestep of 0.25 fs. 20 structures of each pressure (0.1 and 60 MPa, respectively) were produced to obtain good statistical averaging of the following dynamic and structural analyses.

Glass Transition Temperature. To estimate the glass transition temperatures of the prepared glass structures, the structures were first equilibrated for 2.5 ps in the NPT ensemble at 300 K before being subjected to heating to 1500 K with a heating rate of 24 K ps^{-1}. Both steps were performed at 0.1 MPa of pressure for both the glasses quenched at 0.1 and 60 MPa of pressure. Next, the glass transition temperature of all 40 glass structures was evaluated by fitting a line to the low and high-temperature part of the temperature vs simulation cell volume graph, and then estimating the T_g by the intersection of these two lines (see Figure 1d). The T_g of each preparation procedure was now found by taking the average of the measured T_g of the 20 quenches of each quenching type (0.1 and 60 MPa, respectively).

Pore Size Distribution. Pore size distribution analyses were performed using Zeo++[28] with a probe size of 0.7 Å. Presented results are averages of all simulated structures at each designated pressure.

Scattering Functions. Partial radial distribution functions (g_{ij}) were calculated from time-averaged trajectory data at 300 K and the neutron-weighted total radial distribution (g_N) was calculated by[29]

$$g_N(r) = \left(\sum_{i,j=1}^{n} c_i c_j b_i b_j\right)^{-1} \sum_{i,j=1}^{n} c_i c_j b_i b_j g_{ij}(r) \quad (1)$$

where c_i is the fraction of atoms i and b_i is the neutron scattering length of atom type i (6.6460, 6.671, 9.36, and 5.680 fm for C, ^{2}H, N, and Zn, respectively).[30] The g_N (Supporting Information (SI) Figure S11) is both presented in an unbroadened and a broadened version. Broadening was employed according to ref 31 by convolution with a Gaussian distribution with a full width at half-maximum (FWHM) of

$$\mathrm{FWHM} = \frac{5.437}{Q_{max}} \quad (2)$$

where Q_{max} is the maximum recorded wavevector of the experimental spectrum of comparison. We here use Q_{max} = 40 Å^{-1}, which is a common cutoff in neutron experiments. This was done to show the insignificant change of g_N upon densification for a case comparable to what should be measurable. To now compute the structure factor $S(Q)$, first, the partial structure factors ($S_{ij}(Q)$) were computed by

$$S_{ij}(Q) = 1 + \rho_a \int_0^{r_{max}} 4\pi r^2 (g_{ij}(r) - 1) \frac{\sin(Qr)}{Qr} \frac{\sin\left(\frac{\pi r}{r_{max}}\right)}{\frac{\pi r}{r_{max}}} \mathrm{d}r \quad (3)$$

where ρ_a is the atomic number density and r_{max} is the maximum value of the RDF (practically, half the simulation box size). We used the

https://doi.org/10.1021/acs.chemmater.2c00325
Chem. Mater. 2022, 34, 5030−5038

Table 1. Comparisons in the Pressure History Sensitivity of Glass Transition Temperature (T_g) among Different Glass Systems[a]

glass formers	standard T_g (K)	compressed T_g (K)	pressure (GPa)	$\Delta T_g/\Delta P$ (K/GPa)	$(\Delta T_g/\Delta P)/T_g$ (1/GPa)	refs
calcium metaphosphate	790	796	0.5	12	0.02	35
$CaMgSi_2O_6$ (diopside)	982	966	0.5	−32	−0.03	36
alkali borosilicate	843	821	0.5	−44	−0.05	1
silicon	1280	1070	3.7	−57	−0.05	37
glassy water	213	199	0.3	−47	−0.23	38
CH_3COOLi	165	163	0.2	−8.5	−0.05	39
CH_3COONa	156	157	0.15	5.5	0.04	39
CH_3COOK	172	173	0.15	7.0	0.04	39
poly(vinyl chloride)	381	421	0.27	145	0.34	7
polymethylmethacrylate	422	452	0.13	220	0.48	7
polystyrene	408	450	0.13	300	0.67	7
polycarbonate	408	452	0.15	295	0.65	8
ZIF-62	**599**	**559**	**0.06**	**−667**	**−1.19**	**this work**

[a]The T_g values listed above were measured under atmospheric pressure for the hot-compressed glasses.

Lorch function to reduce ripples induced by the finite cutoff of the Fourier transform. The total neutron structure factor was then calculated by

$$S_N(Q) = \left(\sum_{i,j=1}^{n} c_i c_j b_i b_j \right)^{-1} \sum_{i,j=1}^{n} c_i c_j b_i b_j S_{ij}(Q) \quad (4)$$

Persistent Homology Analysis. Persistent homology (PH) was applied to study the structural changes as induced by the applied pressure quenching procedure. A general introduction to PH is found in the Supporting Methods. To characterize the persistence diagrams, we apply the so-called accumulated persistence function (APF) to allow for easy comparison between PDs. The APF is calculated as

$$\mathrm{APF}(t) = \sum_{i:m_i \le t} (d_i - b_i) \quad (5)$$

where t is time; b_i and d_i are the birth and death time of loop i, respectively; and m is the mean age defined by $m_i = (b_i + d_i)/2$. When calculating the topological information, we follow the procedure used in ref 32 using the Diode and Dionysus2 software packages. Estimation of atomic radii follows ref 33, and radii of 0.715, 0.395, 0.625, and 1.575 Å were obtained for carbon, hydrogen, nitrogen, and zinc atoms, respectively. We calculated the persistence diagrams in both dimensions 1 and 2, using an approach where we define the loop as being based on the edges which appears the earliest. The presented spectra are summed for all studied 20 glasses of each preparation technique.

RESULTS AND DISCUSSION

The X-ray diffraction patterns in Figure 1a confirm the crystalline nature of the ZIF-62 sample prepared by the solvothermal method, and the amorphous nature of the two ZIF-62 glass samples that are prepared by melt-quenching (MQ) at ambient pressure (0.1 MPa) and then pressed at 60 MPa (through SPS), respectively. The SPS synthesis conditions are listed in Table S1. As shown in Figure 1b, a significant drop in T_g is observed when 60 MPa of pressure is applied during the SPS densification relative to the ambient pressure synthesis (ΔT_g = 40 K, $\Delta T_g/\Delta P$ = −667 K/GPa). That is, the MQ and SPS ZIF-62 glasses exhibit T_g values of 599 and 559 K, respectively. The microscopic image (Figure S1a) and the DSC curve of the SPS glass powder (Figure S1b) confirm that there are no secondary particles in the SPS ZIF-62 glass, i.e., the T_g drop should be caused by the atomic-scale structural changes. Moreover, by tuning the sintering temperature and pressure, we found that a critical pressure (~50 MPa) is needed, above which the pressure effect on T_g occurs (see details in Supporting Results and Figure S2).

Here, we define the sensitivity parameter of T_g of glass to pressure history as $(\Delta T_g/\Delta P)/T_g$, i.e., the pressure dependence of T_g change is normalized by the ambient pressure T_g value. This parameter can reflect the extrinsic sensitivity of T_g to pressure history for different kinds of glass formers. As shown in Table 1, this value of $(\Delta T_g/\Delta P)/T_g$ for ZIF-62 glass is at least one order of magnitude higher than that of any other glass system with a negative $\Delta T_g/\Delta P$ value.[1,34−39] Notably, subjecting other families of network glasses (e.g., oxide and molecular glasses) to high pressure (0.2~1.0 GPa) leads to both decreasing and increasing T_g, but to a much smaller extent. Notably, various polymer glasses were reported to possess highly positive $(\Delta T_g/\Delta P)/T_g$ values (see Table 1),[7,8] but these values are still much lower than that of the present MOF glass. Thus, the observed drop in T_g indicates that the ZIF-62 structure is hypersensitive to the pressure history compared to other glass systems.

It should be noted that MOF glasses are a new family of glasses featuring network structure and hybrid composition containing both metal nodes and organic ligands. Although it has been reported that pressure history can induce significant changes in the T_g of polymer and inorganic glasses,[1,36] the trend of T_g change with pressure for MOF glasses greatly differs from those of other glass families. Therefore, it is important to reveal the mechanism of the pressure-induced T_g drop for ZIF-62 glass, and thereby to gain new insight into the glass transition in general.

In addition, we note that the T_g values of SPS ZIF-62 glasses in this work were determined under ambient pressure after the pressure quenching cycle, that is, the *ex situ* pressure dependence of T_g. In contrast, the *in situ* pressure dependence of T_g in polymer glasses has been extensively studied.[23,40−42] The *in situ* $\Delta T_g/\Delta P$ values can also reach hundreds of K/GPa.[40,41] However, these $\Delta T_g/\Delta P$ values fundamentally differ from the values reported in Table 1 since the *in situ* values reflect the sensitivity of glass transition dynamics to the *in situ* applied pressure, whereas the *ex situ* values represent the sensitivity of the glass structure to pressure history. Since silica glass possesses network structure consisting of tetrahedral units like the MOF glass, it would be interesting to compare the pressure history effect between them to find the dominant factor for determining T_g. However, to the best of our

https://doi.org/10.1021/acs.chemmater.2c00325
Chem. Mater. 2022, 34, 5030−5038

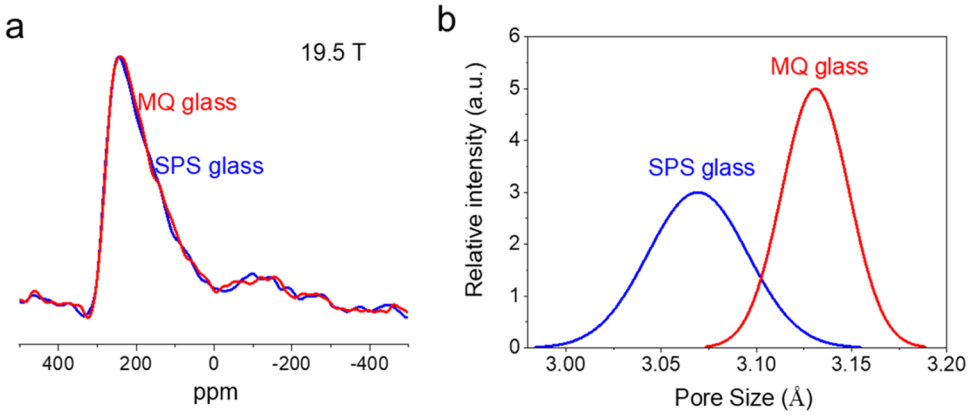

Figure 2. (a) ^{67}Zn NMR spectra collected at 19.5 T for the MQ and SPS ZIF-62 glasses. The SPS glass was sintered at 593 K under 60 MPa. (b) Pore size distribution obtained from the PALS measurements for both studied glasses.

knowledge, the *ex situ* pressure dependence of T_g for silica glass has not been reported and will be an important subject for the future study.

Furthermore, by dynamic and isothermal heating under ambient pressure on the SPS glass (sintered under 60 MPa at 593 K), a striking, fast recovery (i.e., increase from 559 to ∼570 K) of T_g is discovered (see details in Supporting Results and Figures S3 and S4). Similarly, the hardness and density of the SPS glass also recover (i.e., decrease) upon annealing. It implies an intense structural relaxation of the SPS glass upon heat treatment.

To gain insights into the structural origin of the pressure-induced decrease in T_g, we applied a recently developed reactive force field[25] to simulate ZIF-62 glasses. This MD simulation method has been found to reproduce various thermal, mechanical, and structural properties of ZIF glasses in recent studies.[25,26,43] An example structure of ZIF-62 glass produced at ambient pressure is shown in Figure 1c. While the absolute value of the T_g estimated from MD simulations is overpredicted (T_g∼1100 K), the MD simulations correctly predict the large drop (38 K) in T_g with increasing pressure to 60 MPa (Figure 1d), which is close to the experimentally measured T_g drop. The overestimation of the simulated T_g value relative to the measured T_g is typical for all MD simulations of glasses and is commonly ascribed to the high cooling rate. Following the standard approach,[44] T_g is estimated from the inflection point of the calculated simulation cell volume vs temperature curve during heating (Figure 1d). Note that the curves in Figure 1d follow the pattern of the typical volume vs temperature diagram of a glass-forming liquid, with a higher thermal volume expansion found in the liquid compared to the solid state (in the liquid state around 800−1000 ppm K^{-1}, which is on par with numerous other liquids).

Despite the significant changes in T_g, density, and hardness upon densification and annealing, no detectable structural changes occur according to various methods of structural characterizations. In detail, ^{1}H liquid NMR spectra confirm that the organic linker integrity and the linker ratio (Im/bIm) are maintained even after melting under pressure (Figure S5). Raman spectra reveal that the bonding connections within the organic ligands are not affected by the synthesis pressure (Figure S6), and finally, identical Zn 2p and N 1s XPS spectra of the various glasses indicate that the valence bond of the Zn−N coordination bond is retained (Figure S7).

Furthermore, the SR structure of both MQ and SPS ZIF-62 glasses has been probed by ultrahigh-field ^{67}Zn NMR spectroscopy measurements, while their microporosity is determined by PALS. Almost no differences can be detected in the ^{67}Zn NMR spectra of the MQ and SPS ZIF-62 glasses (Figure 2a), implying that the SR disordered structure,[21] i.e., the structure at the scale (<8 Å) of the Zn[ligand]$_4$ tetrahedra, is not affected by the increase in synthesis pressure, and hence the coordination environments remain similar after the SPS treatment. Thus, it is reasonable to infer that the pressure-induced decrease in T_g is not related to the SR structure, unlike the effects of local network connectivity responsible for T_g changes in, e.g., oxide glasses.[22] On the other hand, PALS detects a difference in pore size distribution between MQ and SPS glasses (Figures 2b and S8 and Table S2). MR structural domains, i.e., those at the scale of several Zn[ligand]$_4$ tetrahedra, are involved in the formation of pores with average sizes of about 3.07 ± 0.03 and 3.13 ± 0.02 Å for MQ and SPS glasses, respectively. The PALS results indicate that the pore structure is distorted to some extent upon densification, leading to a decrease in the pore size, which is related to MR structural change. This indicates that the MR structure should be associated with the observed decrease of T_g. That is, distortion of the pore structure produces a more frustrated and energetically excited network structure for SPS glass in comparison to MQ glass. The SPS glass with the more frustrated structure and higher potential energy thus experiences the glass transition at a lower temperature once it is heated.

To further clarify the structural differences between the glasses prepared at different pressures, we have characterized the MD simulation trajectories. First, we examine the Zn coordination number and found it to be 3.52 and 3.53 for the 0.1 and 60 MPa glasses, respectively, in good agreement with the lack of difference in ^{67}Zn NMR spectra. We note that the deviation of the coordination from the tetrahedral configuration is likely induced by the much higher cooling rate in simulations compared to experiments. Similarly, for the average N−Zn−N bond angle, only a minor change from 108.5 to 108.3° is observed upon increasing pressure. Again, this points to SR structure not being responsible for the T_g drop.

To study the MR structural features of the two ZIF-62 glasses, we first calculated the neutron structure factor (Figure 3a), indicating a high degree of overlap for the two samples,

https://doi.org/10.1021/acs.chemmater.2c00325
Chem. Mater. 2022, 34, 5030−5038

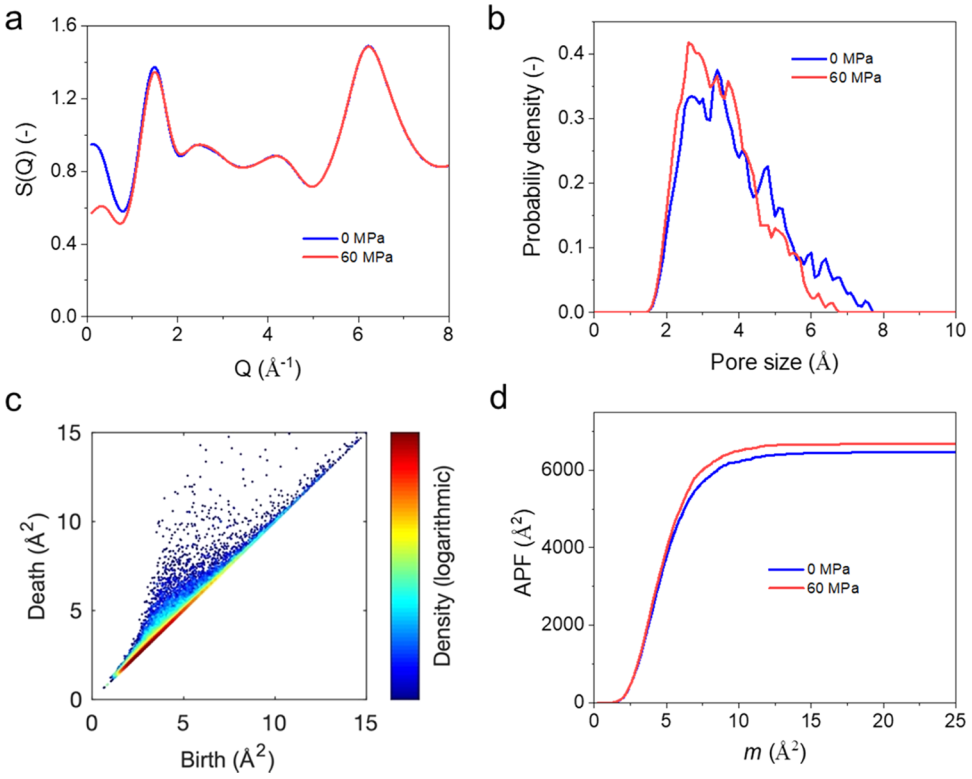

Figure 3. (a) Low-Q region of the neutron structure factor for the simulated ZIF-62 glasses. (b) Pore size distribution of the simulated ZIF-62 glasses. (c) Persistence diagram of voids in the ZIF-62 glass simulated at 0.1 MPa. The corresponding persistence diagram of the ZIF-62 prepared at 60 MPa is presented in Figure S13. The color of each point represents the density of points in its vicinity (from low (blue) to high (red) density). (d) Accumulated persistence function (APF) of persistence diagrams of voids for both 0.1 and 60 MPa ZIF-62 glasses.

except for a slight difference in intensity of the first-sharp diffraction peak ($Q \approx 1.5$ Å^{-1}) and small distortion of the principal peak at $Q \approx 2.5$ Å^{-1}. Furthermore, the change of the small peak at around 0.5 Å^{-1} is found to be caused by the C−C partial structure factor correlation, likely induced by the reorganized packing of the organic moieties within the MOF upon increasing pressure. The partial structure factors, partial radial distribution functions (RDFs) of all atomic pairs, difference RDF plots of 0.1 and 60 MPa structures, as well as the neutron-weighted RDFs are shown in Figures S9−S12, respectively. Generally, all partial structure factors show some pressure-induced changes at low Q values, pointing toward a change in the medium-range structure. For the partial RDFs, only small changes upon pressure treatment are present in the first coordination shell correlations, except for changes in the Zn−Zn correlation extending to beyond >1 nm as also seen in the difference RDF plots of Figure S11. Given the inverse relation between real and reciprocal space, this is consistent with the experimental findings that mainly the MR structure changes with pressure. As the next step, we therefore computed (see the Methods section) and present the pore size distribution in Figure 3b. The average pore sizes for the 0.1 and 60 MPa samples are found to be 3.84 ± 0.30 and 3.50 ± 0.32 Å, respectively, yielding a decrease of ∼0.3 Å upon compression. This difference is close to that observed from the PALS data, although the MD simulations generally yield a slightly larger pore size. The latter is to be expected given the high cooling rate, creating glasses of higher T_g and larger free volume.[45] We also note that there is qualitatively good agreement of the peak positions from the MD-simulated distributions (Figure 3b) and PALS experimental data (Figure 2b).

In an attempt to reveal any nonintuitive, hidden MR structural differences between the samples, we use a method within topological data analysis, namely, persistent homology (see the Supporting Methods section for an introduction to this analysis), to analyze the atomic configuration data from the MD simulations. The basic result of persistent homology is the persistence diagram (PD), which can be obtained for both ring structures (Figure S13) and voids (Figures 3c and S14 for the 0.1 and 60 MPa samples, respectively). Considering first the PDs for rings, a highly scattered diagram is obtained, with a high number of short-lived features around the diagonal, a number of rings that are born early and die late (around the vertical axis), and finally a number of rings in-between these extremes. We note that two intense contributions exist, which are born early ($b \approx 0$) and die at 0.8 and 1.3 Å^2, respectively. These represent the imidazolate and benzimidazolate rings, respectively, as also highlighted in Figure S13. Only small changes with pressure are observed in the ring-based PDs.

To quantify the differences in the PDs for both rings and voids with pressure, we apply the so-called accumulated persistence function (APF),[46] which is an accumulative sum of the lifetime of all topological features in a PD as a function of the mean age. The APF is therefore characterizing all of the features of the PD relevant for understanding glass structure. The APFs for rings of both samples are presented in Figure S15, showing a minor increase in intensity for the 60 MPa structure, which is mainly due to a slightly higher number of rings in this sample. Because the APF is cumulative, its contributions may be split into contributions from different

https://doi.org/10.1021/acs.chemmater.2c00325
Chem. Mater. 2022, 34, 5030−5038

ring sizes. Here, we computed the contributions of rings with three or more atoms to the APFs (Figure S16). We find that the observed differences in APF among the two samples are mainly due to rings containing 3, 6, 8, and >10 atoms. An APF analysis is also performed for the void-based PDs (Figure 3d) of the two structures, showing a slightly higher intensity (caused by more voids) and a minor shift of the inflection point toward lower mean age for the 60 MPa sample (which is also apparent from the normalized APF spectra, Figure S17). The latter suggests that the voids in the structures decrease in size with pressure, in agreement with the pore size distribution determined by simulations (Figure 3b) and measured by PALS (Figure 2b). Considering the PD for long rings (≥ 10 atoms), we find that while the 60 MPa sample features more long loops (~4700 vs ~4900 for 0.1 and 60 MPa, respectively), the long loops of the ambient pressure sample are on average slightly longer (24.3 vs 24.1 atoms for 0.1 and 60 MPa, respectively). We present a histogram of the total distribution of loop sizes in Figure S18. These long rings consist of all atom types, yet with a majority of network percolating species (i.e., C, N, and Zn), suggesting that the connectivity of the network has slightly decreased with increasing pressure.

Finally, we have also performed a Zn-centered PH analysis, for which only the Zn atoms in the structures are considered (Figure S19). This analysis shows a more pronounced decrease in ring size (decrease in lifetime and more points closer to the origin of the PD). Furthermore, a decrease in the average long ring length is observed, from 14.0 to 13.8 atoms upon compression, supporting the decrease in network polymerization and increase of compaction in the percolating Zn-network with increasing pressure.

To address the question of which structural factors govern this significant T_g drop, we have qualitatively reproduced this behavior with reactive MD simulations (Figure 1d). These results imply that pressure leads to considerable structural changes in the ZIF glass framework. The applied pressure during the SPS process induces significant densification in the SPS ZIF-62 glasses, confirmed by the higher density and hardness values relative to those of MQ ZIF-62 glass (Figure S3b). The easy densification induced by the low pressure could be ascribed to two reasons. First, the ZIFs have high structural flexibility[13] caused by the three-dimensional network of small Zn^{2+} ions (~1.2 Å in diameter) and larger organic ligands (Im and bIm are ~4 and ~8 Å in length, respectively). This difference in the size of the structural species leads to freedom for the ligands to rearrange upon compression.[47] Moreover, the large fraction of the organic ligands enhances the flexibility of the ZIF-62 network due to the rotatable organic units.[20] Second, ZIFs have low structural rigidity. Compared to oxide glasses, the rigidity of the ZIF-62 glass is much lower due to the weak coordination Zn−N bonds and the flexible organic ligands.[13] For example, this is reflected in their low hardness and fracture toughness.[26]

The low applied pressure (60 MPa) may neither cause the breakage of the Zn−N bonds nor distort the Zn[ligand]$_4$ tetrahedra. Instead, both PALS measurements (Figure 2b) and MD simulations (Figure 3b−d) reveal a decrease in the pore size and a broader pore size distribution of the ZIF-62 glass prepared under pressure. Although the pore structure of the ZIF-62 crystal becomes disordered upon melting, subnanometer scale cavities are still present in the MQ ZIF-62 glass.[48,49] During the SPS densification process, the application of pressure leads to a collapse of these cavities in the ZIF-62 glass, ultimately densifying the glass structure. Such collapse of cavities leads to changes in MR structure, i.e., reorganization of interconnected Zn[ligand]$_4$ tetrahedral units. The collapse of cavities could lower the degree of the connectivity between the structural units, and hence decrease the polymerization of the glass network. This interpretation is supported by the observed decrease in the average length of long rings upon pressure quenching as found from the persistent homology analysis of the MD trajectories. In this way, T_g decreases intensively with pressure. In addition, the partial recovery of T_g, hardness, and density of the SPS glass upon reheating implies that the glass network connectivity largely recovers during annealing. In contrast to the volume relaxation in compressed oxide glasses,[50] the extent of this volume change in compressed ZIF-62 glass is much greater.

CONCLUSIONS

Through this work, we have gained new insight into the glass transition. It is well known that microstructural (bond strength, cohesive energy, network connectivity) and topological (atomic degree of freedom) factors affect the glass transition behavior. However, in this work, through a detailed study of the pressure history dependence of the glass transition in a MOF glass, we have provided evidence for another critical factor that can highly impact on the glass transition, that is, the pore structure, which relates to the MR structure. The latter is easily altered due to the existence of subnanometer cavities in the glass network, which activate the glass-to-liquid transition when these cavities are slightly compressed and hence distorted. We have shown, through both experiments and simulations, that the distorted subnanometer porous structure is manifested as the decrease in the average size of the pores in ZIF-62 glass.

ASSOCIATED CONTENT

Supporting Information

The Supporting Information is available free of charge at https://pubs.acs.org/doi/10.1021/acs.chemmater.2c00325.

Results of the structural characterizations and simulations (PDF)

AUTHOR INFORMATION

Corresponding Authors

Yuanzheng Yue − *Department of Chemistry and Bioscience, Aalborg University, DK-9220 Aalborg, Denmark;* orcid.org/0000-0002-6048-5236; Email: yy@bio.aau.dk

Morten M. Smedskjaer − *Department of Chemistry and Bioscience, Aalborg University, DK-9220 Aalborg, Denmark;* orcid.org/0000-0003-0476-2021; Email: mos@bio.aau.dk

Authors

Ang Qiao − *Department of Chemistry and Bioscience, Aalborg University, DK-9220 Aalborg, Denmark; State Key Laboratory of Silicate Materials for Architectures, Wuhan University of Technology, Wuhan 430070, China*

Søren S. Sørensen − *Department of Chemistry and Bioscience, Aalborg University, DK-9220 Aalborg, Denmark;* orcid.org/0000-0003-2230-7823

Malwina Stepniewska − *Department of Chemistry and Bioscience, Aalborg University, DK-9220 Aalborg, Denmark*

https://doi.org/10.1021/acs.chemmater.2c00325
Chem. Mater. 2022, 34, 5030−5038

Christophe A. N. Biscio − *Department of Mathematical Sciences, Aalborg University, DK-9220 Aalborg, Denmark*
Lisbeth Fajstrup − *Department of Mathematical Sciences, Aalborg University, DK-9220 Aalborg, Denmark*
Zhu Wang − *School of Physics and Technology, Wuhan University, Wuhan 430072, China*
Xianghua Zhang − *Univ Rennes, CNRS, ISCR (Institut des Sciences Chimiques de Rennes) - UMR 6226, F-35000 Rennes, France;* orcid.org/0000-0002-2180-6543
Laurent Calvez − *Univ Rennes, CNRS, ISCR (Institut des Sciences Chimiques de Rennes) - UMR 6226, F-35000 Rennes, France*
Ivan Hung − *National High Magnetic Field Laboratory, Tallahassee, Florida 32310, United States;* orcid.org/0000-0001-8916-739X
Zhehong Gan − *National High Magnetic Field Laboratory, Tallahassee, Florida 32310, United States;* orcid.org/0000-0002-9855-5113

Complete contact information is available at: https://pubs.acs.org/10.1021/acs.chemmater.2c00325

Author Contributions

[▽]A.Q. and S.S.S. contributed equally to this work.

Notes

The authors declare no competing financial interest.

■ ACKNOWLEDGMENTS

The authors thank VILLUM FONDEN (grant no. 13253) for the support. A.Q. and Z.W. acknowledge National Natural Science Foundation of China (nos. 22175135, 11975169, and U2067207) and the Fundamental Research Funds for the Central Universities (WUT: 2021IVA099, 2021III018JC, and 2021IVB058) for the support. S.S.S. and M.M.S. acknowledge CLAAUDIA for providing computational resources. The authors also thank Sabyasachi Sen from University of California at Davis for valuable discussions.

■ REFERENCES

(1) Wondraczek, L.; Sen, S.; Behrens, H.; Youngman, R. E. Structure-energy map of alkali borosilicate glasses: Effects of pressure and temperature. *Phys. Rev. B* **2007**, *76*, No. 014202.
(2) Kapoor, S.; Wondraczek, L.; Smedskjaer, M. M. Pressure-Induced Densification of Oxide Glasses at the Glass Transition. *Front. Mater.* **2017**, *4*, No. 1.
(3) Atake, T.; Angell, C. Pressure dependence of the glass transition temperature in molecular liquids and plastic crystals. *J. Phys. Chem. A* **1979**, *83*, 3218−3223.
(4) Guerette, M.; Ackerson, M. R.; Thomas, J.; Yuan, F.; Bruce Watson, E.; Walker, D.; Huang, L. Structure and Properties of Silica Glass Densified in Cold Compression and Hot Compression. *Sci. Rep.* **2015**, *5*, No. 15343.
(5) Behrens, H.; Schulze, F. Pressure dependence of melt viscosity in the system $NaAlSi_3O_8$-$CaMgSi_2O_6$. *Am. Mineral.* **2004**, *88*, 1351−1363.
(6) Sheng, H. W.; Liu, H. Z.; Cheng, Y. Q.; Wen, J.; Lee, P. L.; Luo, W. K.; Shastri, S. D.; Ma, E. Polyamorphism in a metallic glass. *Nat. Mater.* **2007**, *6*, 192−197.
(7) Wetton, R. E.; Moneypenny, H. G. Fundamental properties of densified polymeric glasses. *Br. Polym. J.* **1975**, *7*, 51−68.
(8) Holt, A. P.; Fragiadakis, D.; Wollmershauser, J. A.; Feigelson, B. N.; Tyagi, M.; Roland, C. M. Stability Limits of Pressure Densified Polycarbonate Glass. *Macromolecules* **2019**, *52*, 4139−4144.
(9) Schneider, H. A.; Rudolf, B.; Karlou, K.; Cantow, H. J. Pressure influence on the glass transition of polymers and polymer blends. *Polym. Bull.* **1994**, *32*, 645−652.
(10) Williams, E.; Angell, C. Pressure dependence of the glass transition temperature in ionic liquids and solutions. Evidence against free volume theories. *J. Phys. Chem. B* **1977**, *81*, 232−237.
(11) Bennett, T. D.; Tan, J.-C.; Yue, Y. Z.; Baxter, E.; Ducati, C.; Terrill, N. J.; Yeung, H. H.-M.; Zhou, Z.; Chen, W.; Henke, S.; et al.*et al.* Hybrid glasses from strong and fragile metal-organic framework liquids. *Nat. Commun.* **2015**, *6*, No. 8079.
(12) Bennett, T. D.; Yue, Y. Z.; Li, P.; Qiao, A.; Tao, H.; Greaves, N. G.; Richards, T.; Lampronti, G. I.; Redfern, S. A. T.; Blanc, F.; Farha, O. K.; Hupp, J. T.; Cheetham, A. K.; Keen, D. A. Melt-Quenched Glasses of Metal−Organic Frameworks. *J. Am. Chem. Soc.* **2016**, *138*, 3484−3492.
(13) Qiao, A.; Bennett, T. D.; Tao, H.; Krajnc, A.; Mali, G.; Doherty, C. M.; Thornton, A. W.; Mauro, J. C.; Greaves, G. N.; Yue, Y. Z. A metal-organic framework with ultrahigh glass-forming ability. *Sci. Adv.* **2018**, *4*, No. eaao6827.
(14) Horike, S.; Nagarkar, S. S.; Ogawa, T.; Kitagawa, S. A New Dimension for Coordination Polymers and Metal−Organic Frameworks: Towards Functional Glasses and Liquids. *Angew. Chem., Int. Ed.* **2020**, *59*, 6652−6664.
(15) Smedskjaer, M. M.; Sørensen, S. S. A glass act. *Nat. Chem.* **2021**, *13*, 723−724.
(16) Fonseca, J.; Gong, T.; Jiao, L.; Jiang, H.-L. Metal−organic frameworks (MOFs) beyond crystallinity: amorphous MOFs, MOF liquids and MOF glasses. *J. Mater. Chem. A* **2021**, *9*, 10562−10611.
(17) Hayashi, H.; Cote, A. P.; Furukawa, H.; O'Keeffe, M.; Yaghi, O. M. Zeolite A imidazolate frameworks. *Nat. Mater.* **2007**, *6*, 501−506.
(18) Widmer, R. N.; Lampronti, G. I.; Chibani, S.; Wilson, C. W.; Anzellini, S.; Farsang, S.; Kleppe, A. K.; Casati, N. P. M.; MacLeod, S. G.; Redfern, S. A. T.; Coudert, F.-X.; Bennett, T. D. Rich Polymorphism of a Metal−Organic Framework in Pressure−Temperature Space. *J. Am. Chem. Soc.* **2019**, *141*, 9330−9337.
(19) Widmer, R. N.; Lampronti, G. I.; Anzellini, S.; Gaillac, R.; Farsang, S.; Zhou, C.; Belenguer, A. M.; Wilson, C. W.; Palmer, H.; Kleppe, A. K.; Wharmby, M. T.; Yu, X.; Cohen, S. M.; Telfer, S. G.; Redfern, S. A. T.; Coudert, F.-X.; MacLeod, S. G.; Bennett, T. D. Pressure promoted low-temperature melting of metal−organic frameworks. *Nat. Mater.* **2019**, *18*, 370−376.
(20) Bennett, T. D.; Horike, S. Liquid, glass and amorphous solid states of coordination polymers and metal−organic frameworks. *Nat. Rev. Mater.* **2018**, *3*, 431−440.
(21) Madsen, R. S. K.; Qiao, A.; Sen, J.; Hung, I.; Chen, K.; Gan, Z.; Sen, S.; Yue, Y. Z. Ultrahigh-field ^{67}Zn NMR reveals short-range disorder in zeolitic imidazolate framework glasses. *Science* **2020**, *367*, 1473−1476.
(22) Greaves, G. N.; Sen, S. Inorganic glasses, glass-forming liquids and amorphizing solids. *Adv. Phys.* **2007**, *56*, 1−166.
(23) Napolitano, S.; Glynos, E.; Tito, N. B. Glass transition of polymers in bulk, confined geometries, and near interfaces. *Rep. Prog. Phys.* **2017**, *80*, No. 036602.
(24) Zhou, K.; Li, H.; Pang, J.; Wang, Z. Thermal stability of nanocrystalline Cu studied by positron annihilation lifetime spectroscopy and X-ray diffraction. *Philos. Mag.* **2012**, *92*, 2079−2088.
(25) Yang, Y.; Shin, Y. K.; Li, S.; Bennett, T. D.; van Duin, A. C. T.; Mauro, J. C. Enabling Computational Design of ZIFs Using ReaxFF. *J. Phys. Chem. B* **2018**, *122*, 9616−9624.
(26) Sørensen, S. S.; Østergaard, M. B.; Stepniewska, M.; Johra, H.; Yue, Y. Z.; Smedskjaer, M. M. Metal−Organic Framework Glasses Possess Higher Thermal Conductivity than Their Crystalline Counterparts. *ACS Appl. Mater. Interfaces* **2020**, *12*, 18893−18903.
(27) Plimpton, S. Fast Parallel Algorithms for Short-Range Molecular Dynamics. *J. Comput. Phys.* **1995**, *117*, 1−19.
(28) Willems, T. F.; Rycroft, C. H.; Kazi, M.; Meza, J. C.; Haranczyk, M. Algorithms and tools for high-throughput geometry-based analysis of crystalline porous materials. *Microporous Mesoporous Mater.* **2012**, *149*, 134−141.

(29) Keen, D. A. A comparison of various commonly used correlation functions for describing total scattering. *J. Appl. Crystallogr.* **2001**, *34*, 172−177.
(30) Sears, V. F. Neutron scattering lengths and cross sections. *Neutron News* **1992**, *3*, 26−37.
(31) Wright, A. C. Neutron and X-ray amorphography. *J. Non-Cryst. Solids* **1988**, *106*, 1−16.
(32) Sørensen, S. S.; Biscio, C. A. N.; Bauchy, M.; Fajstrup, L.; Smedskjaer, M. M. Revealing hidden medium-range order in amorphous materials using topological data analysis. *Sci. Adv.* **2020**, *6*, No. eabc2320.
(33) Hiraoka, Y.; Nakamura, T.; Hirata, A.; Escolar, E. G.; Matsue, K.; Nishiura, Y. Hierarchical structures of amorphous solids characterized by persistent homology. *Proc. Natl. Acad. Sci. U.S.A.* **2016**, *113*, 7035.
(34) Rzoska, S. J. New Challenges for the Pressure Evolution of the Glass Temperature. *Front. Mater.* **2017**, *4*, No. 33.
(35) Yue, Y. Z.; Wondraczek, L.; Behrens, H.; Deubener, J. Glass transition in an isostatically compressed calcium metaphosphate glass. *J. Chem. Phys.* **2007**, *126*, No. 144902.
(36) Wondraczek, L.; Behrens, H.; Yue, Y. Z.; Deubener, J.; Scherer, G. W. Relaxation and Glass Transition in an Isostatically Compressed Diopside Glass. *J. Am. Ceram. Soc.* **2007**, *90*, 1556−1561.
(37) Deb, S. K.; Wilding, M.; Somayazulu, M.; McMillan, P. F. Pressure-induced amorphization and an amorphous−amorphous transition in densified porous silicon. *Nature* **2001**, *414*, 528−530.
(38) Giovambattista, N.; Loerting, T.; Lukanov, B. R.; Starr, F. W. Interplay of the Glass Transition and the Liquid-Liquid Phase Transition in Water. *Sci. Rep.* **2012**, *2*, No. 390.
(39) Kanno, H.; Shirotani, I.; Minomura, S. Pressure Dependence and Cationic Radius Effect of the Glass Transition Temperature in Aqueous Alkali Acetate Solutions. *Bull. Chem. Soc. Jpn.* **1981**, *54*, 2607−2609.
(40) Tao, R.; Simon, S. L. Pressure-volume-temperature and glass transition behavior of silica/polystyrene nanocomposite. *J. Polym. Sci., Part B: Polym. Phys.* **2015**, *53*, 1131−1138.
(41) Tölle, A. Neutron scattering studies of the model glass formerortho-terphenyl. *Rep. Prog. Phys.* **2001**, *64*, 1473−1532.
(42) Casalini, R.; Roland, C. M. Thermodynamical scaling of the glass transition dynamics. *Phys. Rev. E* **2004**, *69*, No. 062501.
(43) To, T.; Sørensen, S. S.; Stepniewska, M.; Qiao, A.; Jensen, L. R.; Bauchy, M.; Yue, Y. Z.; Smedskjaer, M. M. Fracture toughness of a metal−organic framework glass. *Nat. Commun.* **2020**, *11*, No. 2593.
(44) Morita, H.; Tanaka, K.; Kajiyama, T.; Nishi, T.; Doi, M. Study of the Glass Transition Temperature of Polymer Surface by Coarse-Grained Molecular Dynamics Simulation. *Macromolecules* **2006**, *39*, 6233−6237.
(45) Vollmayr, K.; Kob, W.; Binder, K. How do the properties of a glass depend on the cooling rate? A computer simulation study of a Lennard-Jones system. *J. Chem. Phys.* **1996**, *105*, 4714−4728.
(46) Biscio, C. A. N.; Møller, J. The Accumulated Persistence Function, a New Useful Functional Summary Statistic for Topological Data Analysis, With a View to Brain Artery Trees and Spatial Point Process Applications. *J. Comput. Graph. Stat.* **2019**, *28*, 671−681.
(47) Frentzel-Beyme, L.; Kloß, M.; Kolodzeiski, P.; Pallach, R.; Henke, S. Meltable Mixed-Linker Zeolitic Imidazolate Frameworks and Their Microporous Glasses: From Melting Point Engineering to Selective Hydrocarbon Sorption. *J. Am. Chem. Soc.* **2019**, *141*, 12362−12371.
(48) Thornton, A. W.; Jelfs, K. E.; Konstas, K.; Doherty, C.; Hill, A.; Cheetham, A.; Bennett, T. D. Porosity in metal−organic framework glasses. *Chem. Commun.* **2016**, *52*, 3750−3753.
(49) Frentzel-Beyme, L.; Kloß, M.; Pallach, R.; Salamon, S.; Moldenhauer, H.; Landers, J.; Wende, H.; Debus, J.; Henke, S. Porous purple glass − a cobalt imidazolate glass with accessible porosity from a meltable cobalt imidazolate framework. *J. Mater. Chem. A* **2019**, *7*, 985−990.
(50) Svenson, M. N.; Yougman, R.; Yue, Y. Z.; Rzoska, S. J.; Bockowski, M.; Jensen, L. R.; Smedskjaer, M. M. Volume and Structure Relaxation in Compressed Sodium Borate Glass. *Phys. Chem. Chem. Phys.* **2016**, *18*, 29879−29891.

https://doi.org/10.1021/acs.chemmater.2c00325
Chem. Mater. 2022, 34, 5030−5038